Experimental and Theoretical Characterization of a 40-Gb/s Long-Haul Single-Channel Transmission System

Ronald Holzlöhner, *Student Member, IEEE*, Heider N. Ereifej, *Member, IEEE*, Vladimir S. Grigoryan, *Member, IEEE*, Gary M. Carter, *Member, IEEE*, and Curtis R. Menyuk, *Fellow, IEEE*

***Abstract*—We present a comparison between experiment and simulation of a 40-Gb/s periodically stationary dispersion-managed soliton (DMS) system in a recirculating loop. We find that we can propagate an error-free signal over 6400 km at 40 Gb/s and over 12 000 km if we lower the data rate to 10 Gb/s, keeping all other parameters constant. A careful analysis of the limiting factors shows the strong influence of nonlinear optical pulse-to-pulse interactions, causing a large increase in timing jitter. At a transmission distance of 6400 km, a large fraction of the jitter is due to pulse-to-pulse interactions. Moreover, we find that the system performance is very sensitive to parameter variations. We conclude that periodically stationary DMS systems suffer from numerous problems when increasing the data rate, suggesting that it may be impractical for wavelength-division multiplex transmission at 40 Gb/s.**

***Index Terms*—Amplified spontaneous emission noise, dispersion management, modeling, optical fiber transmission, optical solitons, timing jitter, transmission-line theory.**

I. Introduction

EXTENDING data rates in current optical transmission systems from 10 to 40 Gb/s promises large advantages but also poses great challenges. The sensitivity of the performance to variations in the system parameters is much larger at 40 Gb/s than at 10 Gb/s. There are many complications that appear when increasing the data rate, and careful experimental verification is needed after the system design stage. While there are a number of papers on 40-Gb/s periodically stationary dispersion-managed soliton (DMS) systems [1]–[3], there are few investigations of the underlying physics that limits the transmission distance. In this paper, we compare theory and experiment in a 40-Gb/s recirculating loop of length 107 km. We discuss the optimization of the map design and investigate the system performance as we vary operating parameters such as the optical power, erbium-doped fiber amplifier (EDFA) location, filter bandwidth, and central wavelength. We emphasize that this system does not operate in the quasi-linear DMS regime [4] but at a peak power of about 8 mW, which makes the transmission significantly nonlinear. Moreover, the pulses are approximately periodic with respect to the dispersion map. However, we anticipate some of the results of this work to be relevant to a wider class of systems.

The key detrimental effects that limit the achievable transmission distance in most optical systems are amplitude and timing jitter. Our results show that in our test system, the timing jitter is larger at 40 Gb/s than at 10 Gb/s due to nonlinear optical pulse-to-pulse interactions [5]. This result is significant, since error-free detection is limited to about 5.5 ps of timing jitter in a 10-Gb/s system and to about 1.5 ps at 40 Gb/s [6]. By contrast, we observe that the fluctuation in the pulse energy is about the same at 40 and 10 Gb/s. To make a meaningful comparison and to isolate the impact of pulse-to-pulse interactions on the signal evolution, we prepared our test system to operate in two different modes. In the first mode, we transmitted pseudorandom bit sequences at 40 Gb/s that have a ratio of marks to spaces of 1 : 1, and we will refer to this mode as the 40-Gb/s mode of operation. The second mode is identical to the first, except that the bit pattern was changed to a marks-to-spaces ratio of 1 : 4. There were at least two spaces between each two marks, thereby eliminating pulse-to-pulse interactions. Consequently, the second mode corresponds to transmission at 10 Gb/s while operating with the same pulse parameters, in particular, the same pulse duration and peak power, as the first mode. We will refer to the second mode as the 10_{40} Gb/s mode of operation and stress that it differs from an optimized 10-Gb/s transmission that would use longer pulses and possibly different peak powers.

Measuring and simulating optical timing jitter in a 40-Gb/s system with a precision of under 1 ps is challenging, and the result depends on the exact definition of timing jitter. This paper is one of the first that addresses this complex issue and compares results obtained from different methods in the context of a 40-Gb/s system. We present a detailed study of the jitter evolution and the sources of error in its measurement. In particular, we review the measurement of amplitude and timing jitter using an eye diagram, and, at 10 Gb/s, a method introduced by Mollenauer [7] that relies on the fading of radio-frequency (RF) tones with transmission distance. We then compare the results with the common theoretical definition of timing jitter as a variation in the central pulse time [8]. We show that optical

Manuscript received December 17, 2001. This work was supported in part by the National Science Foundation and in part by the U.S. Department of Energy.

R. Holzlöhner and V. S. Grigoryan are with the Department of Computer Science and Electrical Engineering, University of Maryland Baltimore County, Baltimore, MD 21250 USA (e-mail: holzloehner@umbc.edu).

H. N. Ereifej is with the Laboratory for Physical Sciences, College Park, MD 20740 USA.

G. M. Carter is with the Department of Computer Science and Electrical Engineering, University of Maryland Baltimore County, Baltimore, MD 21250 USA and the Laboratory for Physical Sciences, College Park, MD 20740 USA.

C. R. Menyuk is with the Department of Computer Science and Electrical Engineering, University of Maryland Baltimore County, Baltimore, MD 21250 USA and PhotonEx Corporation, Maynard, MA 01754 USA.

Publisher Item Identifier 10.1109/JLT.2002.800343.

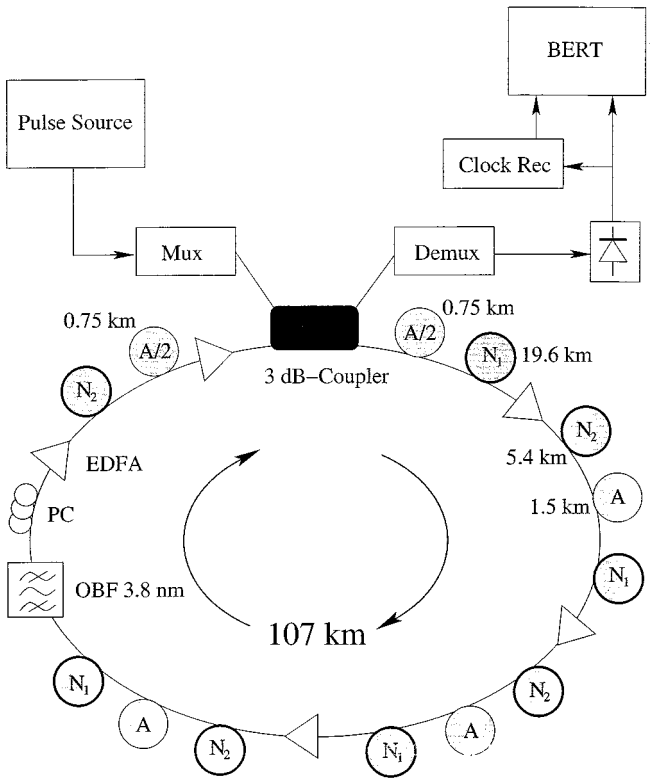

Fig. 1. Simplified experimental setup. The labels A, N_1, and N_2 denote fiber spans of anomalous and normal dispersion, respectively. PC denotes the polarization controller, OBF the inline optical bandpass filter, Clock Rec the clock recovery circuit, and BERT the bit-error-rate tester.

pulse-to-pulse interactions limits the maximum error-free transmission distance at 40 Gb/s to 6400 km. However, our simulations indicate that reducing the length of the dispersion map by 15% would extend the transmission distance to 10 000 km by minimizing the pulse-to-pulse interactions.

The remainder of this paper is organized as follows: In Section II, we describe the experimental setup and the numerical simulation techniques. In Section III, we compare definitions of amplitude and timing jitter and their measurement, discuss dispersion map optimization, and compare the results of experiment and simulation. Section IV contains the conclusions.

II. Experimental Setup and Theory

A. Experimental Setup

We evaluated the transmission performance of our test system both experimentally and through computer simulations. Fig. 1 shows a sketch of the recirculating loop experiment. A mode-locked fiber laser manufactured by PriTel generated the pulses of 4.5-ps full-width half-maximum (FWHM) pulse duration with a repetition rate of 10 GHz. The data stream was modulated at 10 Gb/s with a $2^{23}-1$ pseudorandom bit sequence using a $LiNbO_3$ intensity modulator. The signal was then multiplexed using a two-stage optical time-division multiplexer (TDM), the first one multiplexing the signal up to 20 Gb/s and the second one to 40 Gb/s, by interleaving the 10-Gb/s data stream with a copy of itself that was delayed by about 1 ns. The signal remained unchirped and passed a 3-dB coupler that inserted it into the loop with a peak power of 7.6 mW. All pulses were copolarized. The pulses had a Gaussian shape, and their duration assumed an equilibrium value of $\tau_{\rm opt} = 6$ ps in the loop, measured at the launch point in the map after a few round trips. The average optical power was 1.5 dBm at 40 Gb/s and -3.5 dBm at 10_{40} Gb/s.[1] The center of the launch pulse spectrum lay at 1551.5 nm, while the center of the filter transmission curve was slightly shifted to $\lambda_F = 1551.6$ nm. The offset seemed to help somewhat in shaping the equilibrium pulse but was small compared to the optical bandwidth of about 0.61 nm. The recirculating loop contained four dispersion map periods with a combined length of 106.7 km. Each period of the dispersion map consisted of a 25-km span of normal fiber with dispersion of -1.02 ps/nm-km followed by a 1.5-km span of anomalous fiber with dispersion of 17 ps/nm-km. The path average dispersion was in the range 0.005–0.025 ps/nm-km, depending on λ_F, and the dispersion slope was $dD/d\lambda = 0.0768$ ps/nm^2-km, where D is the local dispersion. Each map period contained an EDFA that divided the normal span into pieces of length 19.6 and 5.4 km, respectively, and we denote the corresponding fiber spans in Fig. 1 by N_1 and N_2. This location minimizes pulse stretching and hence pulse-to-pulse overlap, as we will discuss in Section III-B. The fourth map contained a 3.8-nm optical bandpass filter to reduce the noise, and its anomalous span was split in half by inserting a fifth EDFA, an acoustooptical (AO) loop switch, and the 3-dB coupler in the middle of the span. This map design is based on the 10-Gb/s system described in [9], with the dispersion map length divided by a factor of four. The optical TDM demultiplexer consisted of two stages: an electrooptic $LiNbO_3$ modulator manufactured by Sumitomo that demultiplexed from 40 to 20 Gb/s, and an electroabsorption modulator (JAE) that demultiplexed from 20 to 10 Gb/s.

B. Modeling Setup

We use the scalar split-step method to simulate the light propagation in a time window of 3.2 ns, containing 128 bits at 40 Gb/s and 32 bits at 10 Gb/s. In the recirculating loop that we are modeling, the polarization-dependent loss is about 0.35 dB per round trip and the polarization controllers are optimized to pass the signal with minimum loss, yielding a polarization degree of $>95\%$. Consequently, the polarization orthogonal to the signal is suppressed. In the simulations, as in the experiment, we assume copolarized pulses. We run Monte Carlo simulations in which a different bit sequence is chosen for each realization; the ratio of marks to spaces is always 1 : 1. The EDFAs are modeled as saturable amplifiers with a saturation time of 1 ms and a saturation power of 10 mW. Details on the simulation procedure can be found in [9]. The spontaneous emission factor is $n_{\rm sp} = 1.2$. At the receiver, we include the optical TDM demultiplexer, the clock recovery circuit, and the 20-Gb/s bandwidth-limited photodiode in the simulation model. We note that proper receiver modeling becomes more critical as we go from 10 to 40 Gb/s. For

[1]In order to maintain equal pulse peak powers, we would have had to reduce the average power at 10_{40} Gb/s to $1.5 - 6 = -4.5$ dBm. However, we were not able to lower the EDFA gains that much without increasing $n_{\rm sp}$.

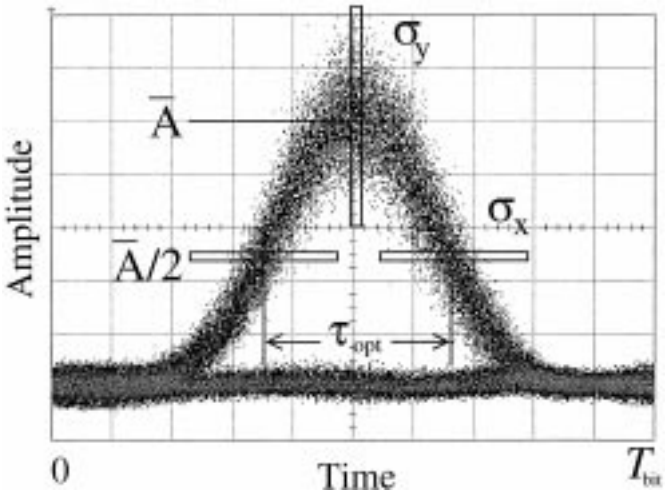

Fig. 2. Schematic of amplitude and timing jitter measurement using a digital oscilloscope. The vertical box is used to measure the absolute amplitude jitter σ_A, and the horizontal boxes are used to measure the absolute timing jitter σ_{t_0}.

example, our 20-GHz photodiode, followed by amplifiers and cables, broadens the received pulses from 6 ps to 23–30 ps, and hence the impulse response of the receiver system has a major influence on the eye diagram. This broadening was not as important in previous 10-Gb/s experiments [9]. We model the effective demultiplexer window function using a Butterworth function $f(t) = 1/[1 + |2(t - t_0)/T_{\mathrm{FWHM}}|^k]$, where t is time, t_0 is the central time of the window, $T_{\mathrm{FWHM}} = 26$ ps is the window duration, and $k = 6.5$ (note that the demultiplexer is not a Butterworth filter, but rather the window function in time happens to follow the Butterworth function). This fitting function is in good agreement with the experimentally measured demultiplexer shape.

III. Results and Discussion

A. Amplitude and Timing Jitter

We find that the values of amplitude and timing jitter depend strongly on the measurement method and that their accurate determination is challenging, in both simulation and experiment. In this section, we will outline the problems we encountered and discuss their solutions.

It is common practice to measure amplitude and timing jitter using the eye diagram on a digital sampling oscilloscope, as shown schematically in Fig. 2. A large number of samples is accumulated in the elongated vertical and horizontal boxes, and the sample histogram as a function of the positions along the long side of the boxes is produced. We denote the mean of the data in the vertical box, which is the mean amplitude, by $\overline{A}$, and the standard deviation of its sample points by σ_y. The difference of the means of the horizontal boxes at amplitude $\overline{A}/2$ is the mean FWHM electrical pulse duration τ, and the symbols $\sigma_{x,l}$ and $\sigma_{x,r}$ denote the standard deviations of the data in the left and right boxes, respectively. Then we define $\sigma_x^2 = (\sigma_{x,l}^2 + \sigma_{x,r}^2)/2$. We call this method of determining the amplitude and timing jitter the scope method.

With the optical field envelope $u(t)$, where t is time, we define the quantities

$$U = \int_0^{T_{\mathrm{bit}}} |u|^2 \, dt \tag{1a}$$

$$t_0 = \frac{1}{U} \int_0^{T_{\mathrm{bit}}} t|u|^2 \, dt \tag{1b}$$

where T_{bit} is the bit duration, U is the pulse energy, and t_0 is the central time of the pulse. If we assume that the pulses after optical filtering and bandwidth-limited square-law detection are Gaussian, so that $|u(t)|^2 = A\exp[-t^2/(2s^2)]$ with an electrical FWHM pulse duration $\tau = 2s\sqrt{2\ln 2}$, then the amplitude is $A = (2U/\tau)\sqrt{\ln 2/\pi}$. We stress again that A depends on τ, and in our system τ is in the range of 23–30 ps, owing to the bandwidth-limited receiver, while the pulse duration in the optical fiber is only $\tau_{\mathrm{opt}} = 6$ ps. This bandwidth limitation makes A a more robust quantity with regard to high-frequency amplified spontaneous emission (ASE) noise that is irrelevant to the detector.

The eye diagram of a signal with finite timing jitter and zero amplitude jitter can have nonzero σ_y; and conversely a signal with finite amplitude jitter and zero timing jitter will yield a nonzero σ_x. In other words, σ_x and σ_y depend in a complicated way on σ_{t_0} and σ_A, the standard deviations of t_0 and A, respectively. We define a dimensionless timing jitter $\Sigma_{t_0} = \sigma_{t_0}/\tau$ [8], where τ is the average FWHM pulse duration. Analogously, we define the dimensionless energy jitter $\Sigma_A = \sigma_A/\overline{A}$, where $\overline{A}$ is the average of the pulse amplitudes A. A first-order approximation, under the assumptions that amplitude and timing fluctuations are statistically independent and τ is constant, is

$$\frac{\Sigma_x}{\Sigma_{t_0}} \approx \sqrt{1 + \left(0.361\frac{\Sigma_A}{\Sigma_{t_0}}\right)^2} \tag{2}$$

where $\Sigma_x = \sigma_x/\tau$. Large ratios of amplitude jitter to timing jitter hence lead to sizable deviations between Σ_x and the relative timing jitter Σ_{t_0}. In our simulations at 10_{40} Gb/s, we obtain after 8400 km the values $\Sigma_A = 7.2\%$, $\sigma_{t_0} = 1.16$ ps, and $\tau = 23$ ps, yielding $\Sigma_x/\Sigma_{t_0} = 1.12$. This jitter enhancement can be even more deceptive when the amount of amplitude jitter in experiments is underestimated due to the common use of deeply saturated electrical amplifiers in the receiver, as discussed in the next section. In (2), the assumption of a constant τ seems to be very strong, and in reality τ fluctuates. However, our experimental timing jitter results are in good agreement with (2), and the approximation serves to show the need for an exact definition of amplitude and timing jitter.

To verify the timing jitter results, we employed a second measurement method that was introduced by Mollenauer and is based on the fading of the RF tones over propagation distance [7]. Due to timing jitter, energy diffuses from the frequency mode at $1/T_{\mathrm{bit}}$ and its harmonics to neighboring frequencies. We expect the normalized timing jitter obtained from this method to be closer to Σ_{t_0} than to Σ_x, and we will show a comparison in the next section.

Amplitude and timing jitter are also enhanced by the optical TDM demultiplexer, whose window function is not square

and thus causes power to leak into adjacent bit slots at the receiver. Even in the absence of pulse leakage, the curvature of the window near the top increases amplitude jitter by attenuating pulses that lie off-center relative to the window.

B. Map Optimization

In this section, we show that the admissible parameter range for transmission of DMS pulses at 40 Gb/s is much smaller than at 10 Gb/s in periodically stationary DMS systems and discuss some of the tradeoffs involved in the parameter optimization.

We consider the dispersion map strength $\gamma = [(\beta_n'' - \beta_{\rm ave}'')L_n - (\beta_a'' - \beta_{\rm ave}'')L_a]/\tau_{\rm opt}^2$, where β_a'', β_n'' and L_a, L_n represent the dispersion values and lengths of the anomalous and normal spans, respectively, $\beta_{\rm ave}'' = (\beta_a'' L_a + \beta_n'' L_n)/(L_a + L_n) = -D_{\rm ave}\lambda_F^2/2\pi c$ is the path average dispersion, and $\tau_{\rm opt}$ is the minimum FWHM pulse duration in the dispersion map [10]. All dispersion values are taken at the central filter wavelength λ_F. In our system, the map strength is $\gamma = 1.95$, corresponding to an energy enhancement of 3.4 and a maximum pulse duration of about 12 ps. As noted in [1], there is a tradeoff in choosing the optimum map strength. Large map strengths and hence stretching factors tend to reduce the Gordon–Haus jitter by a factor on the order of the square root of the enhancement factor [11], [12]. However, if the pulse durations become too large, the pulse tails overlap and start interacting nonlinearly, giving rise to pattern-dependent signal distortion [13], [14], as well as to shifts in the central times of the pulses [15]. The development of ghost pulses that was described in [13] is small in our system at the error-free transmission distances. In our setup, the map strength is slightly larger than optimal, and the nonlinear pulse-to-pulse interactions are our main limiting factor at 40 Gb/s. Earlier work showed that the pulse-to-pulse interactions in a DMS system can be minimized by reducing γ to 1.66 for a value of $T_{\rm bit} \approx 4\tau_{\rm opt}$, where $T_{\rm bit} = 25$ ps is the bit window, equaling the minimum pulse spacing [15]. Our simulations show that by scaling all fiber span lengths by $1.66/1.95 = 0.85$, leading to a dispersion map period of 90 km and an amplifier spacing of 22.6 km, pulse interactions at 40 Gb/s can be removed almost completely and error-free transmission over 10 000 km becomes possible.

In a system with significant nonlinearities, the maximum pulse duration of the pulses in the dispersion map is not determined by the value of γ alone but also strongly depends on the location of the EDFAs in the dispersion map [16]. Fig. 3 shows the evolution of the FWHM pulse duration for one round trip in the recirculating loop. The distance is scaled by the magnitude of the local dispersion so that the anomalous (A) and normal (N) fiber spans appear to have equal lengths. The three curves correspond to placing the EDFAs 0, 5, and 20 km after the beginning of the normal dispersion span, respectively. The corresponding maximum pulse durations are 14.3, 12.5, and 11.6 ps, respectively, at the ends of the normal spans. Our simulations show that the maximum pulse duration is globally minimized when the first four EDFAs are placed at 20 km from the beginnings of the normal dispersion spans. Also, the overall timing jitter at 40 Gb/s is minimized in this case. In the simulations, we also tried to launch the signal at different points in the anomalous span, equivalent to prechirping the pulses. However, we found that launching in the middle of the anomalous span, as was done in the experiments, was optimal.

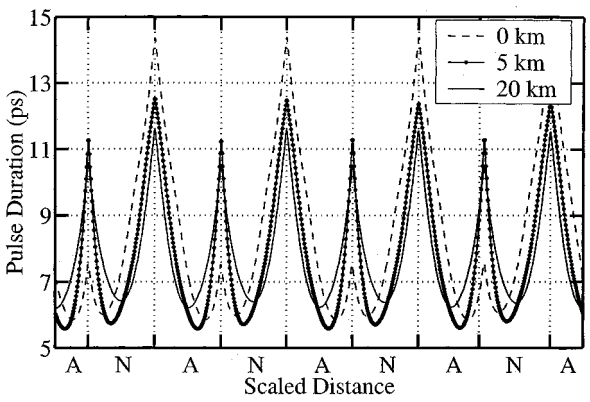

Fig. 3. Evolution of the FWHM pulse duration during one round trip in the recirculating loop for three different EDFA locations in the normal dispersion span. The distance is scaled by the magnitude of the local dispersion so that the anomalous (A) and normal (N) fiber spans appear to have equal lengths.

In the simulations, we observe that neighboring pulses attract each other and tend to reduce their separation in time as they propagate, regardless of their initial phase difference. The pulse-to-pulse attraction is only reduced by 5% when we alternate the phases of adjacent pulses by π, compared to constant phase. This result is consistent with Yu *et al.* [15], who find that the timing jitter is independent of the optical phase when $\gamma \gtrsim 1.65$. (Note that our definition of γ differs from that of Yu *et al.* by a factor of 2.) The physical reason lies in the rapid phase changes due to strong dispersion management. In noise-free simulations of our system, on the other hand, alternating the phase reduces the mutual pulse attraction by as much as 50%, indicating that launching a noise-free phase-alternating signal leads to a mathematically unstable minimum in the pulse attraction.

A tradeoff that is more critical at 40 Gb/s than at 10 Gb/s is the choice of the path average dispersion $D_{\rm ave}$. Larger values of $D_{\rm ave}$ keep the entire pulse spectral range in the anomalous dispersion regime, which tends to stabilize the soliton pulse shapes. On the other hand, the timing jitter grows with $D_{\rm ave}$. Although we can achieve an optimum transmission distance of 18 000 km at 10_{40} Gb/s with $D_{\rm ave} \approx 0.03$ ps/nm-km, this dispersion value is too large at 40 Gb/s due to the increased sensitivity to timing jitter. A similar tradeoff applies to the optimum optical peak power. On one hand, a higher peak power improves the optical signal-to-noise ratio, but on the other hand, it enhances nonlinear pulse-to-pulse interactions.

C. Comparison of Simulation and Experiment

In the experiment, we optimized the loop parameters to achieve the maximum transmission distance at 40 Gb/s. To isolate the impact of nonlinear pulse-to-pulse interactions, we then compared the 40-Gb/s system to a system at the reduced data rate of 10 Gb/s while keeping all other parameters constant, denoted by 10_{40} Gb/s. In particular, we still used the optical TDM demultiplexer at 10_{40} Gb/s. Therefore, our 10_{40} Gb/s transmission was almost identical to the 40-Gb/s case, except that the minimum pulse spacing was 100 ps.

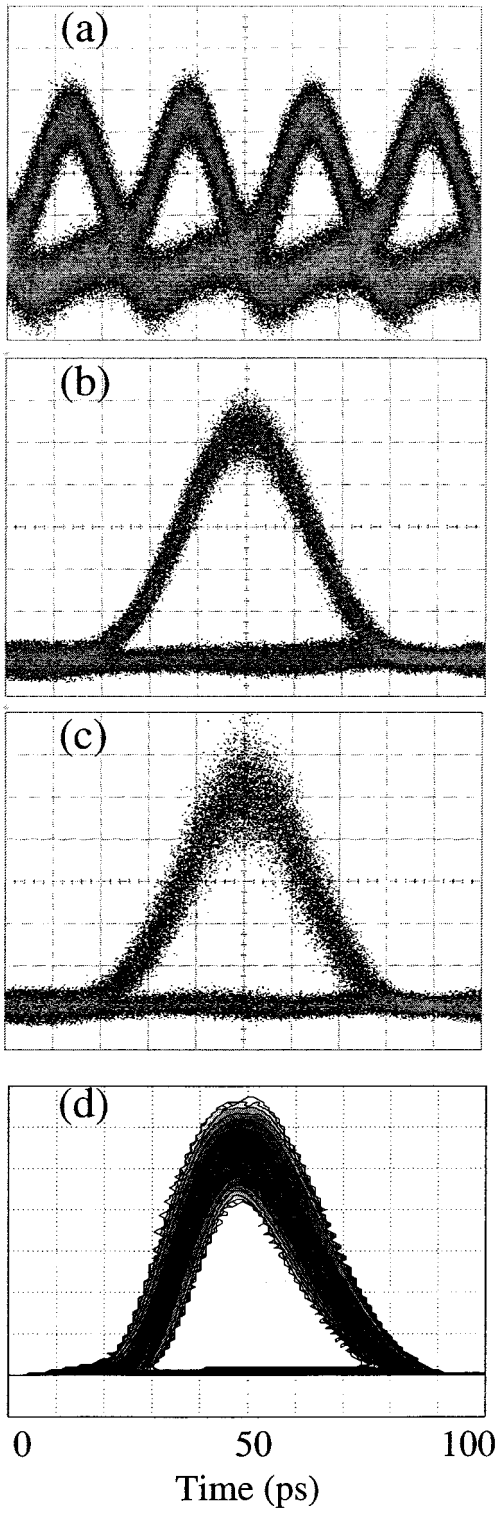

Fig. 4. (a) Input pulse train at 40 Gb/s, measured with a 40-GHz photodiode. (b) Eye diagram of a pulse after 0 km (back-to-back) at 40 Gb/s measured at the output of a 20-GHz photodiode. (c) Eye diagram of a pulse after 6000-km propagation. (d) Contour plot of probability densities of the simulated photodiode current.

Fig. 4 shows the eye diagram at 40 Gb/s without using electrical narrow-band filters. Fig. 4(a) shows the 40-Gb/s pulse train before it is inserted into the loop, using a 40-Gb/s monitor photodiode. This photodiode has a high electrical bandwidth,

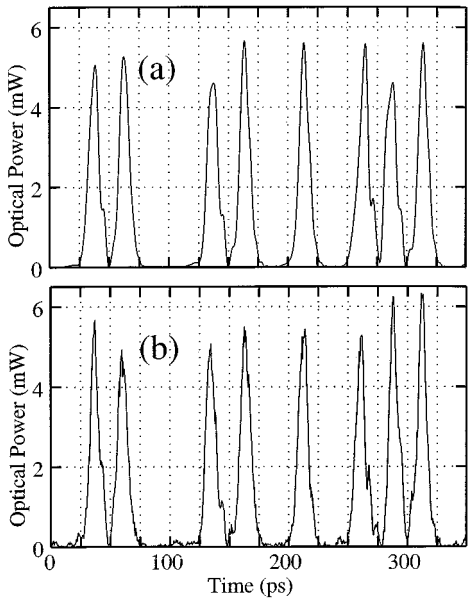

Fig. 5. Optical power at 40 Gb/s after 6400 km at the maximum expansion point in the map. Simulation (a) without ASE noise and (b) with noise. The noise-free signal in (a) shows a strong pulse distortion that is entirely due to pulse-to-pulse interactions.

but it also produces a large amount of electrical noise. Therefore, we did not use it to measure eye diagrams. Fig. 4(b) and (c) shows the eye diagrams of a single pulse in the demultiplexed signal at 0 km and 6400 km, respectively, using a 20-Gb/s photodiode. No electrical filtering was applied to the signal. Fig. 4(d) shows the simulated eye diagram in the form of a contour plot. The slightly asymmetrical pulse shape is due to the electrical modeling of the bandwidth-limited photodiode.

Fig. 5 shows the optical power in the 40-Gb/s simulations after 6400 km. The data were extracted after the normal fiber span, where pulses are maximally expanded, corresponding to the location of the four largest peaks in Fig. 3. Comparing Fig. 5(a), where the ASE noise was turned off in all the EDFAs, with Fig. 5(b) being with the noise turned on, we observe that a large part of the pulse distortion is present in the absence of noise. Isolated pulses, such as the fifth pulse in (a), all evolve identically when the ASE noise input is turned off; hence, this distortion must be due to pulse-to-pulse interactions. The peak power fluctuation in (a) is mostly due to the significant pulse shape distortion and does not imply a large pulse energy fluctuation Σ_A. Instead, Σ_A is mostly caused by noise and is about six times larger in (b) than in (a). Note also that the noise in the zeros in (b) is small.

Fig. 6 shows the timing jitter evolution at 40 Gb/s and at 10_{40} Gb/s for both experiment and simulation using the scope method, where the crosses and circles show the experimental and the curves show the numerical results. In the simulations, we emulate the statistical function of the digital oscilloscope described in Section III-A using Monte Carlo simulations, rather than using the central time definition of the timing jitter. The initial jitter of about 0.2 ps is due to our suboptimal demultiplexing, leading to the leakage of neighboring pulses into the demultiplexer window. Error-free data transmission breaks down after 6400 km at 40 Gb/s and after 12 000 km at 10_{40} Gb/s.

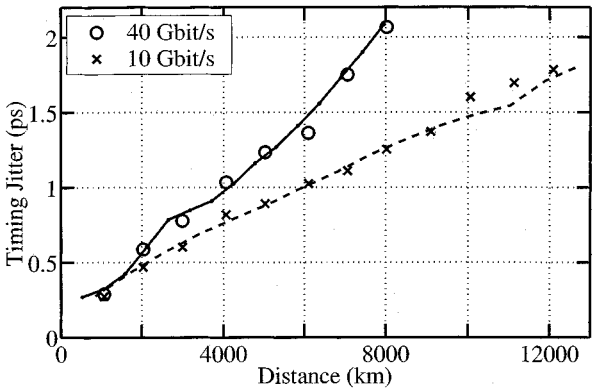

Fig. 6. Timing jitter at 40 and 10_{40} Gb/s using the scope method. The circles and crosses show the experimental measurement, and the lines show the simulation results.

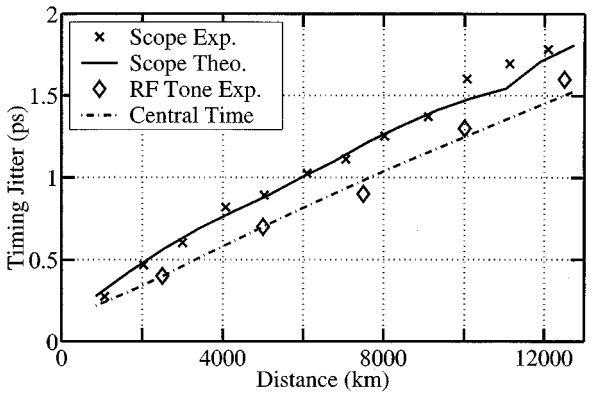

Fig. 8. Comparison of the scope method and the RF tone fading method at 10_{40} Gb/s to highlight jitter enhancement.

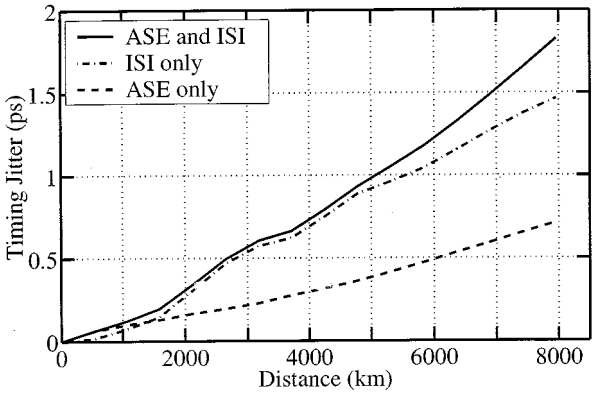

Fig. 7. Timing jitter contributions in the 40-Gb/s simulation with a perfect (square) demultiplexer window. All curves show timing jitter according to the central time definition. Solid line: full simulation. Dash-dotted line: no ASE noise ($n_{\rm sp} = 0$), exhibiting pulse-to-pulse interactions only. Dashed line: timing jitter with ASE noise, but with the bit pattern $101010\cdots$ instead of a random bit pattern, therefore removing pulse-to-pulse interactions.

The reduced timing jitter at 10_{40} Gb/s is due to the absence of pulse-to-pulse interactions. Note that $n_{\rm sp}$ is slightly larger at 10_{40} Gb/s than at 40 Gb/s; the two curves would diverge even further with equal values of $n_{\rm sp}$. The breakdown of the transmission occurs in two stages: a first stage at 6400–7500 km, in which the error rate exceeds 10^{-9} mainly due to timing jitter; and a second stage beyond 7500 km, where the pulses themselves break down due to pulse-to-pulse distortion and ASE noise. The present system is limited by timing jitter, not by noise in the zeros, as was the case in earlier 10-Gb/s experiments [9]. As a consequence, the bandwidth and exact filter profile of the optical inline filter are of less importance. We varied filter types and the filter bandwidth between 2.8 and 4.6 nm without observing large differences in the maximum transmission distance. If we were able to extend the transmission at 40 Gb/s to distances beyond 12 000 km, our previous modeling [16] shows that DMS robustness would critically depend on the optimization of the inline filter.

Fig. 7 compares the evolution of the jitter of the central time Σ_{t_0} in the simulations for three different cases; we used an ideal (square) demultiplexer window to eliminate eye degradation due to the demultiplexer. The solid curve shows the timing jitter resulting from the full simulations, including ASE noise, at 40 Gb/s. The dash-dotted line shows the same timing jitter in the absence of ASE noise, exhibiting the effect of pulse-to-pulse interactions only. The dashed line is the timing jitter with ASE noise, but with the alternating bit pattern $101010\ldots$ instead of a random bit pattern, thereby removing the pulse-to-pulse interactions. The latter procedure allows a more accurate isolation of pulse-to-pulse effects than reducing the data rate to 10_{40} Gb/s, since the average power in the loop is kept strictly constant in the presence of saturable EDFAs. Again, one can see the significant impact of pulse-to-pulse interactions on the timing jitter. However, the fact that the curves for the noisy and noise-free signals are so close does not mean that noise is negligible in this system. Weak noise breaks the unrealistic perfect phase symmetry between adjacent pulses and might mitigate their mutual attraction in the beginning, while at larger distances increasing the timing jitter. According to [13] and [17], pulse-to-pulse attraction due to intrachannel cross-phase modulation (XPM) depends on the ratio $x = \tau_{\rm opt}/T_{\rm bit}$, where $\tau_{\rm opt}$ is the optical FWHM pulse duration and $T_{\rm bit}$ is the bit duration. The magnitude of the attraction is proportional to $\exp(-1/2x^2)/x^3$. This function has an extremely steep slope for $0.3 < x < 1$. The maximum value that x assumes during the first loop revolution is $x = \tau_{\rm opt}/T_{\rm bit} = 12$ ps/25 ps $= 0.48$, resulting in a pulse-to-pulse attraction of 8.7% relative to its maximum near $x = 1$. This attraction is only effective over the short range in the map where the pulse duration is close to its maximum; see Fig. 3. However, once the pulses approach each other, the effective $T_{\rm bit}$ is reduced, the ratio x increases, and hence the attraction grows very fast.

In Fig. 8, we show the timing jitter σ_x measured by the scope using crosses and the results of the RF tone measurement using diamonds. Since the bandwidth of our electrical equipment is limited to about 40 Gb/s, we can only apply the RF tone method to 10_{40} Gb/s transmission [5]. The solid line represents the simulation result of the absolute timing jitter from the scope method σ_x, while the dashed line shows the simulation result of σ_{t_0} (central time method). The difference between the curves amounts to 10–20%, depending on the amplitude jitter at each data point, and agrees with (2). On the other hand, note the good agreement between the RF tone method and σ_{t_0}.

Fig. 9 exhibits the squared normalized energy variance Σ_A^2 in the 40 Gb/s and 10_{40} Gb/s simulations. The dashed line is a

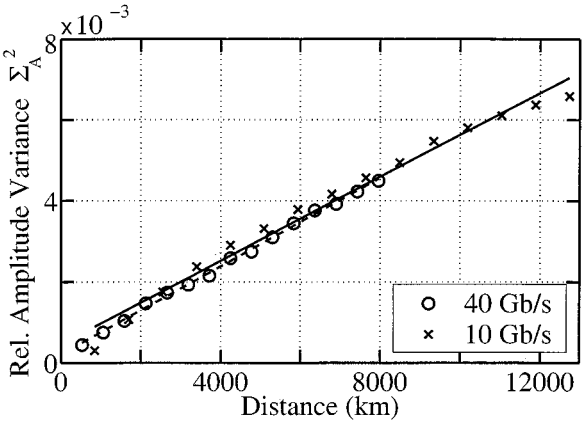

Fig. 9. Relative energy variance, Σ_A^2, in the 40- and 10_{40}-Gb/s simulations. The dashed line is a linear fit to the measured results at 40 Gb/s, and the lines are fits to the 10_{40}-Gb/s results.

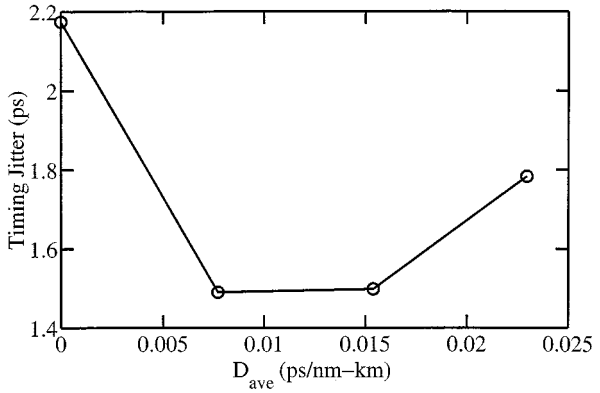

Fig. 10. Dependence of the timing jitter on the path-average dispersion $D_{\rm ave}$ at 40 Gb/s after 6400 km. The wavelength is increased by 0.1 nm for each data point.

linear fit to the measured results at 40 Gb/s and the solid line to the 10_{40}-Gb/s results. The values at 40 Gb/s and 10_{40} Gb/s are almost identical, indicating that little energy is transferred between pulses when they interact nonlinearly, and the energy jitter is mainly due to ASE noise energy that grows linearly with distance [8]. We found that the impact of energy jitter can easily be underestimated due to the use of saturated electrical amplifiers. Our Anritsu RF amplifier, located between the photodiode and the bit error rate tester (BERT), is deeply saturated and hence compresses the rail of the ones in the eye diagram compared to the zeros rail. Electrical amplifier saturation, in contrast to EDFA saturation, is a very fast process and hence distorts the signal shape. For this reason, we only used the RF amplifier to drive the BERT and not to produce any eye diagrams.

To highlight the sensitivity of the system to variations in the path-average dispersion, we simulated the signal propagation at different wavelengths. Fig. 10 shows the timing jitter as a function of $D_{\rm ave}$ at 6400 km. The data points correspond to a wavelength spacing of 0.1 nm, and the 40-Gb/s simulation was performed at $D_{\rm ave} = 0.0154$ ps/nm-km. Although we have not attempted WDM transmission in the recirculating loop, it is obvious that the present third-order dispersion of $dD/d\lambda = 0.0768$ ps/nm^2-km is large enough to spread different channels over a large range of $D_{\rm ave}$, resulting in increased timing

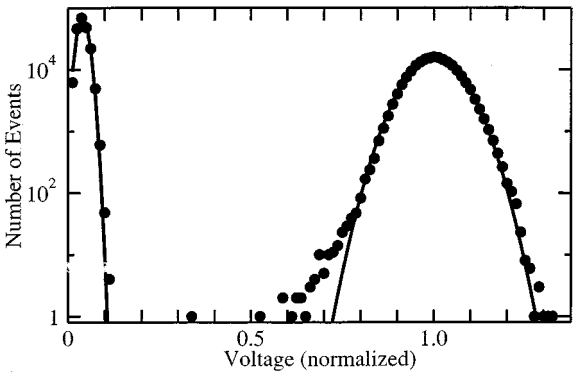

Fig. 11. Histogram of the narrow-band filtered receiver voltage at 40 Gb/s, resulting from the Monte Carlo simulation at a propagation distance of 7500 km. The left peak corresponds to the spaces, the right peak to the marks. The solid lines are Gaussian fits. The departure from the Gaussian behavior is obvious in the tails.

jitter in the edge channels. Our simulation shows that even in single-channel transmission, the third-order dispersion strongly deteriorates the signal and hence has to be taken into account, in contrast to previous 10-Gb/s systems with wider pulses [9]. The physical reason is that third-order dispersion leads to asymmetrical pulses; in the present 40-Gb/s system, the leading tails of the pulses are stretched out and interact with adjacent pulses.

Fig. 11 shows a histogram of the received voltage after narrow-band filtering at 40 Gb/s, obtained from the Monte Carlo simulation of 3000 realizations. The propagation distance is 7500 km, which is about 1200 km beyond the distance where error-free transmission breaks down. The solid lines are Gaussian fits to the data points, using their mean and variance. The Q-factor based on the Gaussian fits is still larger than six, indicating error-free transmission. However, due to the departure of the probability density from Gaussian shape, the true error rate exceeds 10^{-9}, as is the case in the experiment. We note that the distortion of the Gaussian distribution in Fig. 11 is so severe that even a fit to only the data points that are part of the low voltage tail of the distribution of the marks fails.

IV. Conclusions

We demonstrate good agreement between experiment and simulation of a 40-Gb/s periodically stationary dispersion-managed soliton system in a recirculating loop. We use periodic dispersion compensation and a 3.8-nm optical inline filter. Reducing the data rate to 10 Gb/s, while keeping all other parameters constant, we are able to isolate the impact of the nonlinear pulse-to-pulse interaction, and we find that it is the key limiting effect at 40 Gb/s. The simulation enables us to optimize path-average dispersion, optical power, and amplifier spacing within the normal dispersion fiber span, all of which have strong impact on the maximum transmission distance. Of lesser influence on the error-free transmission distance are the optical inline filter bandwidth, the precise pulse shape at the launch point for a given pulse duration, and a small initial wavelength offset between the launched signal spectrum and the transmission maximum of the optical inline bandpass filter. The simulation shows that our dispersion map strength of 1.95 is slightly larger than optimal and that error-free transmission

at 40 Gb/s can be extended to 10 000 km if we reduce the length of our map period by 15%. We emphasize that timing jitter and the pulse-to-pulse interactions are strongly coupled in our loop and limit the propagation distance. The accurate experimental determination of both the amplitude and the timing jitter is not simple, and we compare different definitions and measurement methods. In conclusion, we find that the system is very sensitive to changes in the system parameters and conclude that the periodically stationary DMS format may not be practical for WDM transmission at 40 Gb/s.

ACKNOWLEDGMENT

The authors thank J. Zweck and B. Marks for inspiring discussions and substantial help with the manuscript.

REFERENCES

[1] I. Morita, K. Tanaka, N. Edagawa, and M. Suzuki, "40 Gb/s single-channel soliton transmission over transoceanic distances by reducing Gordon–Haus timing jitter and soliton–soliton interaction," *J. Lightwave Technol.*, vol. 17, pp. 2506–2511, 1999.

[2] K. Suzuki, H. Kubota, A. Sahara, and M. Nakazawa, "40 Gbit/s single channel optical soliton transmission over 70 000 km using inline synchronous modulation and optical filtering," *Electron. Lett.*, vol. 34, pp. 98–100, 1998.

[3] G. Aubin, T. Montalant, J. Moulu, F. Pirio, J.-B. Thomine, and F. Devaux, "40 Gb/s OTDM soliton transmission over transoceanic distances," *Electron. Lett.*, vol. 32, pp. 2188–2189, 1996.

[4] F. Le Guen, S. Del Burgo, M. L. Moulinard, D. Grot, M. Henry, F. Favre, and T. Georges, "Narrow band 1.02 Tbit/s (51×20 Gbit/s) soliton DWDM transmission over 1000 km of standard fiber with 100 km amplifier spans," in *Proc. OFC'99*, Washington, DC, 1999, paper PD4.

[5] H. N. Ereifej, R. Holzlöhner, and G. M. Carter, "Inter-symbol interference and timing jitter measurements in a 40 Gb/s long-haul dispersion-managed soliton system," IEEE Photon. Technol. Lett., to be published.

[6] J. P. Gordon and H. A. Haus, "Random walk of coherently amplified solitons in optical fiber transmission," *Opt. Lett.*, vol. 11, pp. 665–667, 1986.

[7] L. F. Mollenauer, M. J. Neubelt, S. G. Evangelides, J. P. Gordon, and L. G. Cohen, "Experimental study of soliton transmission over more than 10 000 km in dispersion-shifted fiber," *Opt. Lett.*, vol. 15, pp. 1203–1205, 1990.

[8] V. S. Grigoryan, C. R. Menyuk, and R.-M. Mu, "Calculation of timing and amplitude jitter in dispersion-managed optical fiber communications using linearization," *J. Lightwave Technol.*, vol. 17, pp. 1347–1356, 1999.

[9] R.-M. Mu, V. S. Grigoryan, C. R. Menyuk, G. M. Carter, and J. M. Jacob, "Comparison of theory and experiment for dispersion-managed solitons in a recirculating fiber loop," *IEEE J. Select. Topics Quantum Electron.*, vol. 6, pp. 248–257, 2000.

[10] N. J. Smith, N. J. Doran, F. M. Knox, and W. Forysiak, "Energy-scaling characteristics of solitons in strongly dispersion-managed fibers," *Opt. Lett.*, vol. 21, pp. 1981–1983, 1996.

[11] N. J. Smith, N. J. Forysiak, and W. Doran, "Reduced Gordon–Haus jitter due to enhanced power solitons in strongly dispersion managed systems," *Electron. Lett.*, vol. 32, pp. 2085–2086, 1996.

[12] G. M. Carter, J. M. Jacob, C. R. Menyuk, E. A. Golovchenko, and A. N. Pillipetskii, "Timing-jitter reduction for a dispersion-managed soliton system: experimental evidence," *Opt. Lett.*, vol. 22, pp. 513–515, 1997.

[13] P. V. Mamyshev and N. A. Mamysheva, "Pulse-overlapped dispersion-managed data transmission and intrachannel four-wave mixing," *Opt. Lett.*, vol. 24, pp. 1454–1456, 1999.

[14] M. J. Ablowitz and T. Hirooka, "Resonant nonlinear intrachannel interactions in strongly dispersion-managed systems," *Opt. Lett.*, vol. 25, pp. 1750–1752, 2000.

[15] T. Yu, E. A. Golovchenko, A. N. Pilipetskii, and C. R. Menyuk, "Dispersion-managed soliton interactions in optical fibers," *Opt. Lett.*, vol. 22, pp. 793–795, 1997.

[16] V. S. Grigoryan, P. Sinha, C. R. Menyuk, G. M. Carter, and A. Hasegawa, "Long distance transmission of filtered dispersion-managed solitons at 40 Gb/s bit systems rate over 6400 km," in *1999 ROSC Symposium on Massive WDM and TDM Soliton Transmission*, A. Hasegawa, Ed. New York: Kluwer, 1999.

[17] J. Mårtensson, A. Berntson, M. Westlund, A. Danielsson, P. Johannisson, D. Anderson, and M. Lisak, "Timing jitter owing to intrachannel pulse interactions in dispersion-managed transmission systems," *Opt. Lett.*, vol. 26, pp. 55–57, 2001.

Ronald Holzlöhner (S'00) was born in Essen, Germany, on December 30, 1970. He received the M.S. degree in physics from the Technical University of Berlin, Germany, in 1998. He is currently pursuing the Ph.D. degree at the University of Maryland Baltimore County (UMBC).

He studied at the University of California, Santa Barbara, in 1995/1996 as a Fulbright Exchange Student. While at UMBC, he works part-time as a Consultant for Virtual Photonics, Inc. (Website: http://www.photonics.umbc.edu/.)

Heider N. Ereifej, photograph and biography not available at the time of publication.

Vladimir S. Grigoryan, photograph and biography not available at the time of publication.

Gary M. Carter, photograph and biography not available at the time of publication.

Curtis R. Menyuk (SM'88–F'98) was born March 26, 1954. He received the B.S. and M.S. degrees from the Massachusetts Institute of Technology, Cambridge, in 1976 and the Ph.D. degree from the University of California, Los Angeles, in 1981.

He has worked as a Research Associate at the University of Maryland, College Park, and at Science Applications International Corporation, McLean, VA. In 1986, he became an Associate Professor in the Department of Electrical Engineering at the University of Maryland Baltimore County (UMBC), Baltimore, and he was the founding member of the department. In 1993, he was promoted to Professor. He has been on partial leave from UMBC since 1996. From 1996 to 2001, he worked part-time for the Department of Defense (DoD), codirecting the Optical Networking Program at the DoD Laboratory for Telecommunications Sciences, Adelphi, MD, from 1999 to 2001. In August 2001, he left the DoD and became Chief Scientist at PhotonEx Corporation, Maynard MA. For the last 15 years, his primary research interest has been theoretical and computational studies of fiber-optic communications. He has authored or coauthored more than 140 archival journal publications as well as numerous other publications and presentations. He has also edited two books. The equations and algorithms that he and his research group at UMBC have developed to model optical fiber transmission systems are used extensively in the telecommunications industry.

Dr. Menyuk is a Fellow of the Optical Society of America (OSA) and a member of the Society for Industrial and Applied Mathematics and the American Physical Society. He is a former UMBC Presidential Research Professor.